Journal of Hydrology 610 (2022) 127978

Contents lists available at ScienceDirect

Journal of Hydrology

journal homepage: www.elsevier.com/locate/jhydrol

Research papers

Comparison of a laser precipitation monitor, piezoelectric transducer and particle imaging transient visual measurement technology under simulated rainfall in laboratory conditions

Enshuai Shen [a,b], Gang Liu [a,b,*], Mohamed A.M. Abd Elbasit [c], Xiaoyun Zhan [a,b], Qian Feng [a], Chenxi Dan [a], Hongqiang Shi [a], Xiangyu Chen [a], Qiong Zhang [a], Zhen Guo [d]

[a] State Key Laboratory of Soil Erosion and Dryland Farming on the Loess Plateau, Institute of Soil and Water Conservation, Northwest A&F University, Yangling 712100, China
[b] Institute of Soil and Water Conservation, Chinese Academy of Sciences and Ministry of Water Resources, Yangling 712100, China
[c] Department of Physical and Earth Sciences, Sol Plaatje University, Kimberley 8301, South Africa
[d] Sichuan Huabiaoce Testing Technology Co. Ltd., Chengdu, Sichuan 610097, China

ARTICLE INFO

This manuscript was handled by Marco Borga, Editor-in-Chief, with the assistance of Francesco Marra, Associate Editor

Keywords:
Rainfall intensity
Raindrop size distribution
Rainfall kinetic energy
Rainfall erosivity
Raindrop microphysics

ABSTRACT

Precipitation microphysics, which describes the basic characteristics of rainfall, is important for agricultural praxis, weather prediction, aviation safety, and soil erosion prediction. In this study, three types of instruments (a laser precipitation monitor, LPM; piezoelectric transducer, PT; and particle imaging transient visual measurement technology, PIV) were employed to measure and compare the raindrop size distribution (DSD) and rainfall kinetic energy rate (KE_t) under simulated rainfall conditions. Comparisons of the results indicated that under the same simulated rainfall conditions, the number of raindrops per unit area measured by LPM was larger than that measured by PIV. The DSD measured by PIV was more uniform than that of the PT and LPM under the same rainfall conditions. The raindrop size range measured by the LPM was smaller than that measured by the PT and PIV. In addition, the geometric mean diameter was a more accurate representation of raindrop size because PIV can capture the true irregular shape of raindrops. Compared to the PIV sensor, the LPM underestimates the raindrop diameter. The median raindrop diameter measured and calculated by PIV using the geometric mean diameter was approximately 1.61 times that of LPM. The KE_t values measured by PIV and PT were approximately similar, while the KE_t calculated by LPM was 0.51 and 0.57 times that of PIV and PT for the same rainfall conditions, respectively. A correction factor of 1.75 provided an approximate reference for the calibration of the kinetic energy calculation of the LPM instrument. The above results can provide basic insights for calibration and application of the three instruments.

1. Introduction

Raindrop characteristics provide fundamental information on precipitation microphysics, which play a significant role in many aspects, such as rainfall prediction, agricultural praxis, canopy interception, and artificial precipitation (Bassette and Bussière, 2008; Frasson and Krajewski, 2011; Lanza and Stagi, 2008; Liu et al., 2019a; Ma et al., 2019; Guo et al., 2015; Szakall et al., 2009; Stagnaro et al., 2021; Zhan et al., 2018). Rain is also an important weather factor affecting aircraft flight safety, and the collisions between raindrops and aircraft wings can cause aircraft flight energy loss (Zhang and Cao, 2010). In addition, raindrop splash erosion plays a vital role in water erosion processes (Xiao et al., 2017). Splash erosion is affected directly by the microphysical properties of rainfall, such as raindrop size distribution (DSD), terminal velocity, rainfall intensity, rainfall kinetic energy (KE) and momentum (Abd Elbasit et al., 2010; Carollo et al., 2016; Hu et al., 2016; Xiao et al., 2017).

The KE is a rainfall variable used to describe rainfall characteristics (Abd Elbasit et al., 2010; Carollo et al., 2017; Fischer et al., 2016; Shen et al., 2021a; Shen et al., 2021b; Van Dijk et al., 2002). Some researchers have used a single raindrop diameter and raindrop terminal velocity to calculate KE (Abd Elbasit et al., 2011; Angulo-Martinez et al., 2016;

* Corresponding author at: Institute of Soil and Water Conservation, Northwest A&F University, No. 26, Xinong Road, Yangling, Shaanxi Province 712100, China.
E-mail address: gliu@foxmail.com (G. Liu).

https://doi.org/10.1016/j.jhydrol.2022.127978
Received 12 February 2022; Received in revised form 19 May 2022; Accepted 22 May 2022
Available online 28 May 2022

Fornis et al., 2005; Meshesha et al., 2016; Zhan et al., 2018). KE can be defined as half of the product of the mass and the square of the velocity of the raindrops (Abd Elbasit et al., 2011; Meshesha et al., 2016; Zhan et al., 2018). The total KE is the sum of the KE of single raindrops calculated by the diameter and the corresponding fall terminal velocity (Sharma et al., 1995; Salles et al., 2002; Serio et al., 2019). Numerous scholars have estimated KE empirically based on its relationship to rainfall intensity (Angulo-Martinez et al., 2016; Meshesha et al., 2016; Wilken et al., 2018). However, this relationship varies with geographical locations, climate regimes, and rain types (Meshesha et al., 2016; Ma et al., 2019; Lanza et al., 2021). Therefore, reliable methods to calculate the KE were measured directly by rainfall instruments. To calculate KE, the DSD and terminal velocity of each raindrop must be known. DSD data have been obtained by using various traditional methods, such as the staining method, filter paper, flour pellet method and infiltration method (Abd Elbasit et al., 2011; Guo et al., 2015; Park et al., 1983; Salles et al., 2002; Shin et al., 2016). However, the traditional methods have some deficiencies, including the inability to perform continuous measurements and inconvenient operation (Johannsen et al., 2020; Zhan et al., 2018). Various rainfall measurement instruments have been developed based on different principles to directly measure DSD continuously during rainfall events due to advances in technology and electronics (Lanza et al., 2021). The Joss-Waldvogel disdrometer was the first automatic instrument to measure the sizes of raindrops based on the vertical component of the raindrop momentum (Chang et al., 2020; Joss and Waldvogel, 1967; Liu et al., 2019a). Piezoelectric transducers (PTs) measure the DSD and KE based on acoustic principles (Abd Elbasit et al., 2010; Abd Elbasit et al., 2011). Other optical disdrometers have also been developed (Carollo et al., 2018; Loffler-Mang and Joss, 2000). For example, the particle measurement system uses the light array arrangement method to observe raindrop characteristics (Meshesha et al., 2016). The optical spectro-pluviometer applies infrared radiation light LED (0.9-μm wavelength) technology to observe raindrops falling through a parallel beam (Salles et al., 1998; Wilken et al., 2018). On the other hand, laser precipitation monitor (LPM) utilizes infrared light to directly measure the DSD and the corresponding fall velocity (Liu et al., 2019a). In addition, a 2D video disdrometer, hydrometer velocity and shape detector were integrated as an electronic optical device to record the two- or three-dimensional shape, size, and fall velocity of raindrops (Chang et al., 2020; Kruger and Krajewski, 2002; Liu et al., 2019b). Other instruments that using radar for measurement have also been developed to monitor raindrop characteristics, such as those using microrain radar (Chang et al., 2020; Liu et al., 2019b; Ma et al., 2019). Additionally, particle imaging transient visual technology (PIV), which depends on a charge-coupled device camera that takes pictures of raindrops and records their size and duration, was developed (Guo et al., 2015). PIV can be used to accurately obtain the microphysical characteristic parameters of raindrops associated with the shape of a single raindrop. Zhan et al. (2018) used PIV to measure the DSD and calculate the fall terminal velocity of natural raindrops and found that the rainfall KE calculated by PIV was more accurate than that of previous empirical models. As various rainfall measurement instruments are widely used, appropriate studies are needed to determine their performance and suitability (Lanza et al., 2021). Many researchers have compared various noncatching types of instruments used to measure raindrop properties. Chang et al. (2020) showed that microrain radar was superior to other instruments by comparing the uncertainty and accuracy of four types of measuring DSD instruments (microrain radar, Joss-Waldvogel disdrometer, 2D-video disdrometer, and precipitation occurrence sensor system). Krajewski et al. (2006) reported that the DSD and rainfall amounts measured by three types of disdrometers were relatively different under natural rainfall conditions. Tokay et al. (2001) found that the rainfall measured by a 2D video disdrometer is more accurate than that measured by the Joss-Waldvogel disdrometer (JWD). Guillermo et al. (2016) concluded that PWS100 could provide more reliable data for rainfall measurement by comparing two optical instruments (a light beam occlusion type, OAP-2DP and a light scatter sensor, PWS100). However, for noncatching instruments, there is a lack of accurate calibration and standard calibration procedures (Lanza et al., 2021). Studies that compare various rain instruments with different systems and methods under the same calibration and evaluation conditions are needed. The measured raindrop characteristics of these types of instruments, especially the LPM, PT, and PIV, have never been evaluated and compared under the same rainfall conditions.

The aims of this study were i) to compare the abilities of LPM, PT, and PIV to measure KE and DSD; ii) to evaluate the advantages and disadvantages of the LPM, PT, and PIV under the same rainfall conditions; and iii) to provide some guidelines for the application of the LPM, PT, and PIV. The results of this study can provide insights into the basic rainfall characteristic measurements.

2. Materials and methods

2.1. Instruments

2.1.1. Laser precipitation monitor (LPM)

An LPM (Thies Clima, Germany, Fig. 1a) is an optical disdrometer. It has a laser-optical ray generator and can generate an infrared rectangular light band with an area of 45.6 cm^2 (Fig. 1b). When raindrops pass through the laser rectangular area, the detector receives a weakened signal. According to the amplitude and duration of the signal reduction, the diameter and falling velocity of the raindrops can be computed (Adolf Thies and Co, 2011).

The disdrometer data were recorded and compiled by using LPM View 2.7 software, which can export one-minute of DSD data. The output data include the number of raindrops, rainfall amount (mm), rainfall intensity (mm h^{-1}), raindrop diameter (mm) and corresponding fall velocity (m s^{-1}). The raindrop diameter is divided into 23 classes ranging from 0.125 to 8.5 mm, and the raindrop fall velocity is divided into 20 classes ranging from 0.2 to 11 mm s^{-1} for each minute. Assuming that the raindrops are spherical, the mass of the raindrops is calculated using the measured raindrop diameter (Meshesha et al., 2016). Then raindrop KE is computed based on the raindrop mass and falling velocity measurements.

2.1.2. Piezoelectric transducer (PT)

A PT sensor consists of two separate sensors (Fig. 2), which are

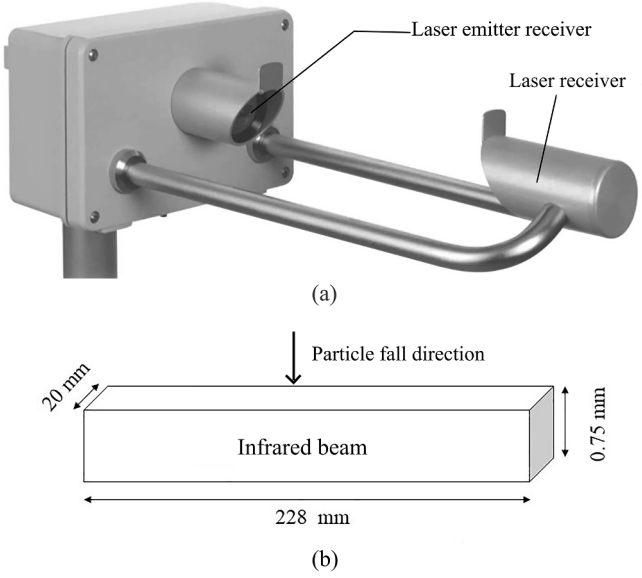

Fig. 1. (a) Picture and (b) particle measurement schematic of the laser precipitation monitor.

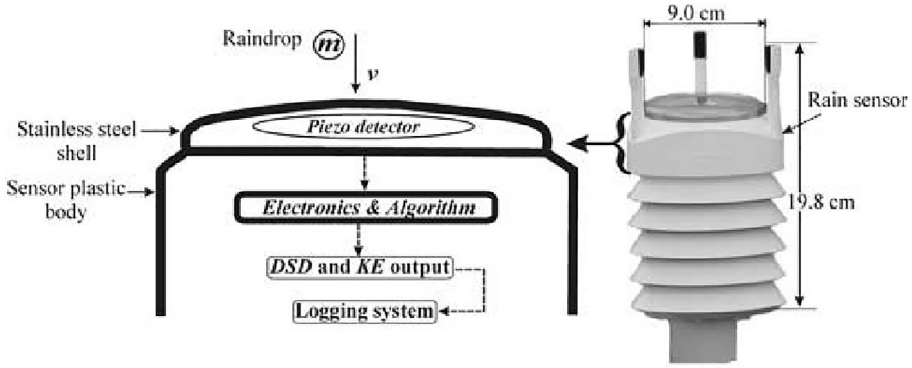

Fig. 2. The working principle and a picture of piezoelectric transducers (the figure is from Abd Elbasit et al., 2010).

modified from a Vaisala RAINCAP rainfall sensor (Abd Elbasit et al., 2011). Each sensor is composed of a detector made of piezoelectric material and a stainless-steel shell. The measurement area is 60 cm^2. One of the two sensors (PT-KE) is used to measure the rainfall KE, and the other sensor (PT-DSD) is used to measure the rainfall DSD. The principle of the PT sensor relies on the ability of a crystal plate to generate electrical charges when it receives a raindrop impact force (Abd Elbasit et al., 2011).

The PT sensor is based on detecting the acoustic effects of individual raindrops. The impact force of a raindrop generates sound waves that the sensor detects, and the mechanical stress generated by sound waves in the sensor causes the sensor electrodes to generate a voltage. The change between the voltage signals is determined by the raindrop impact, which can be used to determine the raindrop KE and diameter. Meanwhile, to improve the accuracy of the measurement, the sensor adopts noise filtering technology to eliminate signals from sources other than the initial raindrop impact. Before the signals are recorded, different electronic systems are used to filter, amplify, digitize and analyse the signals generated by the sensor elements (Abd Elbasit et al., 2010; Abd Elbasit et al., 2011). Abd Elbasit et al. (2011) verified PT-DSD and PT-KE sensor output data and found that the two sensors have a significant relationship under different rainfall intensities. A more detailed description of the instrument can be found in Abd Elbasit et al. (2010); Abd Elbasit et al. (2011).

The PT sensors are connected to two computers via an RS-232 serial interface, taking ten seconds as the recording interval. The raindrop diameter is divided into 8 classes ranging from 1 to 5 mm, which are normalized to the mean drop size (Table 1). According to the configuration of the sensor, the output of each raindrop size class is the number of raindrops and the KE.

2.1.3. Particle imaging transient visual measurement technology (PIV)

PIV was developed to identify raindrops based on particle imaging visual measurement technology (Guo et al., 2015; Zhan et al., 2020). It consists of the following three subsystems: a projection subsystem, an acquisition subsystem, and an acquisition control subsystem (Fig. 3). A charge-coupled device (CCD) industrial camera (BASLER acA 1920-150 μm, 1920 × 1200 pixels, Germany) is used to collect digital images of raindrops on the projection screen. The frame rate of the camera was 480 frames s^{-1}, and the exposure time was 1/500 s. When a raindrop entered the measurement area, the state of each raindrop was recorded by the CCD industrial camera to determine its spatial position and shape in a specific time series. Then, raindrop image interpretation system software is employed to process the raindrop images and calculate the raindrop size and fall velocity. The original raindrop image size is corrected by computer vision recognition technology, the excess noise is eliminated by computer image depth processing, and then the binarized raindrop image is outlined. Based on the distance difference of the homologous raindrop images and the exposure time of the camera, the raindrop fall velocity is calculated. This PIV measured the raindrop diameter within a range of 0.17–8 mm (Zhan et al., 2020). In this system, an area-scan CCD camera rather than a line-scan camera was chosen so that images were captured continuously, and virtual slides of panoramic images were completed in real time (Zhan et al., 2020). For each rainfall event, the PIV can be measured continuously, and the raindrop sampling interval is one minute. Meanwhile, the interpretation software can export the one-minute raindrop diameter and the corresponding raindrop velocity. A detailed description of the PIV instrument can be found in Zhan et al. (2020).

To test the accuracy of PIV, Guo et al. (2015) compared the measured diameter and falling velocity of a steel ball with the actual and known diameter and theoretical falling velocity of the steel ball and verified that PIV could effectively and rapidly measure the microphysical characteristics of raindrops (Guo et al., 2015; Zhan et al., 2018, Zhan et al., 2020).

Table 1
Raindrop size classes of the piezoelectric transducer sensor (Abd Elbasit et al., 2010).

Class	Raindrop size range (mm)	Mean raindrop size (mm)
1	0.80–1.12	1.00
2	1.12–1.40	1.25
3	1.40–1.79	1.60
4	1.79–2.24	2.00
5	2.24–2.89	2.50
6	2.89–3.59	3.20
7	3.59–4.49	4.00
8	> 4.49	5.00

2.2. Experimental design

The experiments were conducted under simulated rainfall at the State Key Laboratory of Soil Erosion and Dryland Farming on the Loess Plateau in Yangling, China. The spatial distribution uniformity of natural rainfall is not controllable because of wind and geographic locations. Therefore, a rainfall simulator with downwards sprinkler nozzles was applied to simulate rainfall and the raindrops with a certain initial velocity ejected by the downwards rainfall simulator. The downwards sprinkler nozzles of the rainfall simulator were set 18 m above the three instruments so that all measured raindrops in this study could reach their terminal velocity. The uniformity of the simulated rainfall was >85%. However, due to the limitation regarding the ability of simulators to simulate rainfall uniformly, 10 different simulator sprinkler nozzles with various aperture size (0–45%) were adjusted to regulate the size and number of raindrops with different rainfall intensities. The gradient of each sprinkler nozzle aperture size adjustment was 5%. The mean rainfall intensity of the 10 groups of different sprinkler nozzle aperture sizes ranged from 45.6 mm h^{-1} to 157.2 mm h^{-1} (Table 2).

First, three instruments, an LPM, PT, and PIV, were placed in a

Fig. 3. The PIV components. (a) General views and (b) a schematic view of the particle imaging visual measurement principles (Zhan et al., 2020). CCD camera = charge-coupled device camera.

Table 2
Raindrop diameters and numbers from the laser precipitation monitor (LPM) and particle imaging transient visual measurement technology (PIV) for 10 groups of different rainfall intensities.

Rainfall intensity (mm h^{-1})	Number of raindrops per unit area (n/m^2)		D_{50} (mm)		Min. diameter (mm)		Max. diameter (mm)	
	LPM	PIV	LPM	PIV	LPM	PIV	LPM	PIV
45.6	334,912	203,900	0.82	1.27	0.13	0.17	2.50	3.58
64.8	4,576,096	300,125	0.83	1.27	0.13	0.17	2.50	3.63
76.8	5,015,351	392,500	0.84	1.27	0.13	0.17	2.50	3.91
94.8	5,948,684	449,650	0.81	1.32	0.13	0.17	2.50	3.61
105.6	6,783,114	513,350	0.86	1.36	0.13	0.17	2.50	3.87
129	7,164,474	560,125	0.87	1.41	0.13	0.17	3.00	3.61
135.6	7,164,912	593,775	0.90	1.53	0.13	0.17	3.50	4.49
144	6,791,009	573,775	0.99	1.67	0.13	0.17	3.00	4.43
150	6,805,921	571,425	1.12	1.87	0.13	0.17	3.50	4.54
157.2	7,209,430	585,075	1.40	2.20	0.13	0.17	4.00	4.84

Note: D_{50} = median raindrop diameter.

uniform rainfall area (Fig. 4). The experiments were run when the rainfall intensity was stable. Meanwhile, four computers were employed to simultaneously record the data. To obtain optimal DSD and raindrop fall velocity results, the three instruments were tested continuously and simultaneously for 10 min at each aperture size of the sprinkler nozzles.

The rainfall intensity was measured with a tipping bucket rain gauge connected to an event recorder (Onset HOBO RG3-M, USA). The gauge automatically flips when the rainfall amount reaches 0.2 mm and automatically records the numbers of flips. Finally, computer software (HOBO ware Pro 3.7.12) was used to filter and export the rainfall data and compute the rainfall intensity at different time intervals.

2.3. Data analysis

2.3.1. Laser precipitation monitor (LPM)

The raindrop parameters, including the raindrop diameter and fall velocity, were measured and recorded as the primary LPM sensor output. The rainfall kinetic energy rate (KE_t) was then computed using the integral function of the entire raindrop spectrum in a time interval (Liu et al., 2019b).

$$KE_t = (\frac{\rho\pi}{12}) \times (\frac{1}{10^6}) \times (\frac{3600}{t_{LPM}}) \times (\frac{1}{A_{LPM}}) \times \sum n_i \bullet d_i^3 \bullet v_{di}^2 \quad (1)$$

where KE_t is the rainfall kinetic energy rate (J $m^{-2}h^{-1}$); ρ is the density of water (kg m^{-3}); t_{LPM} is the measurement time interval of the LPM (60 s); A_{LPM} is the measurement area of the LPM sensor (0.00456 m^2); n_i is the drop count in the drop spectrum raster cell i; d_i is the mean drop diameter of drop spectrum class i (mm); and v_{di} is the actual measured fall terminal velocity of the drop with a diameter of d_i (m s^{-1}).

2.3.2. Piezoelectric transducers (PT)

The KE_t from the PT-KE sensor was calculated using the following equation (Abd Elbasit et al., 2011):

$$KE_t = \left(\frac{3600}{t_{PT}}\right) \bullet \left(\frac{10^4}{A_{PT}}\right) \bullet \sum_{i=1}^{n} KE_i \quad (2)$$

where t_{PT} is the measurement time interval of the PT (10 s); A_{PT} is the area of the measurement piezoelectric sensor (60 cm^2); n is the number of classes; and KE_i is the kinetic energy measured for class $i = 1$–8 (mJ).

The PT-DSD sensor measures the number of raindrops in each class (1–8, Table 1), so the DSD of raindrops can be used to calculate KE_t using the following equations (Salles et al., 2002; Abd Elbasit et al., 2011):

$$KE_t = (\frac{\rho\pi}{12}) \times (\frac{1}{10^6}) \times (\frac{3600}{t_{PT}}) \times (\frac{1}{A_{PT}}) \times \sum n_i \bullet d_i^3 \bullet v_{di}^2 \quad (3)$$

The raindrop falling velocity without wind for the PT-DSD sensor was computed by using the following equation (Abd Elbasit et al., 2011):

$$v_{di} = 3.78 \times d_i^{0.67} \quad (4)$$

where d_i is the raindrop diameter in each class (mm).

2.3.3. Particle imaging transient visual measurement technology (PIV)

The raindrop diameter derived from PIV adopts the geometric mean diameter. The calculation method is based on the two points with the longest raindrop contour distance. This distance is taken as the maximum raindrop diameter (Fig. 5, D1). A vertical line was drawn through the midpoint of the maximum diameter (Fig. 5, D2). The vertical line distance between two points on the contour is the minor-axis diameter of the raindrop. The geometric mean of the maximum diameter and the minor-axis diameter is the geometric mean diameter of the raindrops (D) (Zhan et al., 2020).

$$D = \sqrt{D_1 \times D_2} \quad (5)$$

where D is the geometric mean diameter of the raindrops (mm); D_1 is the length of the long axis (mm); and D_2 is the length of the short axis (mm).

The following formula was used to calculate the falling velocity of the raindrops (Zhan et al., 2020):

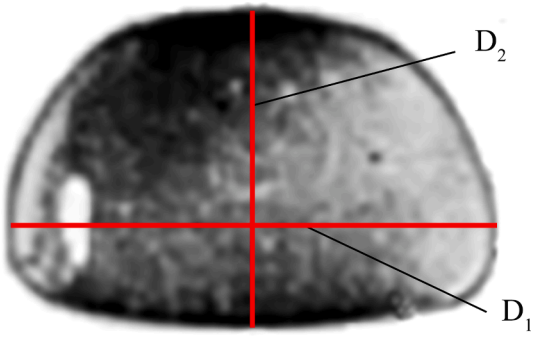

Fig. 5. Schematic view of a single raindrop measured by using PIV sensors. D_1 and D_2 represent the major and minor axes, respectively.

Fig. 4. General view of the experimental area and sensor setup under the rainfall simulator showing the three investigated sensors, tipping bucket rain gauge and recording rain shelter.

$$V_D = \frac{10^{-3}(L-D)}{t} \quad (6)$$

where V_D is the falling velocity of the raindrops (m s^{-1}); L is the trailing length of the raindrops (mm); and t is the exposure time of the camera (s).

KE_t is calculated based on a single raindrop diameter and falling velocity by using the following formula (Salles et al., 2002; Abd Elbasit et al., 2011; Zhan et al., 2020):

$$KE_t = \left(\frac{\rho\pi}{12}\right) \times \left(\frac{1}{10^6}\right) \times \left(\frac{3600}{t_{PIV}}\right) \times \left(\frac{1}{A_{PIV}}\right) \times \sum D^3 \bullet V_D^2 \quad (7)$$

where t_{PIV} is the measurement time interval of PIV (60 s) and A_{PIV} is the measurement area of PIV (0.04 m^2).

2.3.4. Statistical analysis

All statistical analyses were performed using R 3.6.2 and Excel 2016. The determination coefficient (R^2) was applied to evaluate the appropriateness of the regression equations. To ensure that the measurement intervals of the three instruments were the same, all the calculations were based on data recorded during a one minute period. All rainfall data from the beginning to the end were used to calculate the average rainfall intensity, KE_t, and raindrop diameter characteristic information.

3. Results

3.1. Raindrop number and size

As shown in Table 2, LPM measured more raindrops per unit area than PIV for cases with the same rainfall intensity (Table 2). The number and size of raindrops measured by LPM and PIV under the same rainfall conditions were significantly different. For all tested rainfall intensity cases, the median raindrop diameters (D_{50}) measured using LPM and PIV ranged from 0.82 to 1.40 mm and 1.27–2.20 mm, respectively (Table 2). In this study, the PIV-measured D_{50} was 1.51–1.7 times that of the LPM, with an average value of 1.61 times (Table 2). The former was smaller than the latter, and both increased with increasing rainfall intensity. The minimum diameters measured by the LPM and PIV were 0.13 mm and 0.17 mm, respectively (Table 2). The maximum diameters measured by the LPM and PIV ranged from 2.50 to 4.00 mm and 3.58–4.84 mm, respectively (Table 2). It could be concluded that the raindrop size range measured by PIV was larger than that measured by the LPM for cases with the same rainfall.

3.2. Raindrop size distribution (DSD)

The shaded area in Fig. 6 represents the DSD ranges under 10 different rainfall intensities, and the dashed line shows the largest and smallest rainfall intensities. The raindrop size ranges measured by LPM, PT and PIV were 0.13–3.5 mm, 0.8–4 mm and 0.17–4.49 mm, respectively, for the 10 raindrop distributions. This result indicates that the three instruments obtain different minimum and maximum raindrop diameters measurements for each rainfall event. The raindrop sizes measured by the LPM, PT-DSD, and PIV were primarily distributed in the ranges of < 1.5 mm, 1–2 mm, and < 2 mm, respectively. However, the proportions of small raindrops (<1 mm) measured by the LPM, PT-DSD, and PIV were 97%, 7% and 80%, respectively. The raindrop size distribution measured by PIV was more uniform than that measured by

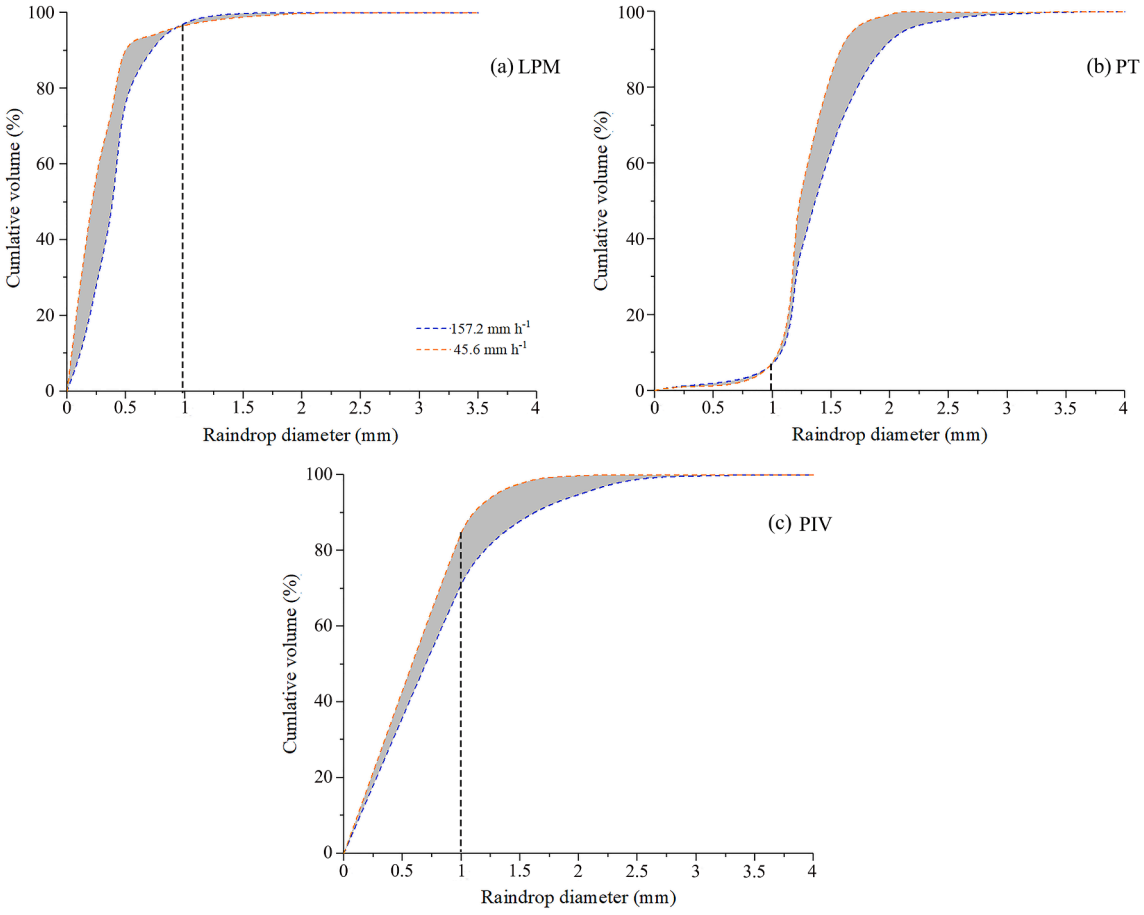

Fig. 6. Raindrop size distribution range measured by (a) a laser precipitation monitor (LPM), (b) a piezoelectric transducer (PT), and (c) particle imaging transient visual measurement technology (PIV) under 10 different rainfall intensities in the range of 45.6–157.2 mm h^{-1}.

PT and LPM under the same rainfall conditions (Fig. 6).

3.3. Raindrop fall velocity

The falling velocity and diameter of raindrops measured by the LPM and PIV increased with increasing rainfall intensity. Meanwhile, the falling velocity of raindrops measured by the LPM and PIV increased with increasing raindrop diameter (Fig. 7). The velocity distribution of raindrops and DSD for the lightest rainfall intensity (45.6 mm h^{-1}) measured by the LPM was similar to that measured by PIV and was different for both the moderate (105.6 mm h^{-1}) and large (157.2 mm h^{-1}) rainfall intensities. Under the same rainfall conditions, the falling velocity of < 1 mm raindrops measured by the LPM was greater than that of PIV, while for the > 1 mm raindrops, the opposite was true.

3.4. Rainfall kinetic energy (KE_t)

For 10 different rainfall intensities, the KE_t values measured by the LPM were in the range of 73.63–187.22 J $m^{-2}h^{-1}$; those measured by PT-KE were in the range of 132.80–392.22 J $m^{-2}h^{-1}$; those measured by PT-DSD were in the range of 122.88–367.44 J $m^{-2}h^{-1}$; and those measured by PIV were in the range of 129.34–298.95 J $m^{-2}h^{-1}$. The KE_t measured by the three instruments increased with increasing rainfall intensity, and the relationships could be described by exponential functions (Fig. 8). It could also be observed that the KE_t measured by LPM was significantly smaller than that those measured by PT and PIV. Fig. 9 shows a good linear relationship between the directly measured KE_t by using PT-KE and the estimated KE_t by using PT-DSD. This result indicates that the KE_t measured by PT-KE and that measured by PT-DSD were approximately consistent.

The KE_t measured by PT was approximately 1.1 times that measured by PIV (Fig. 10a, b). The KE_t of the LPM was approximately 0.57 times

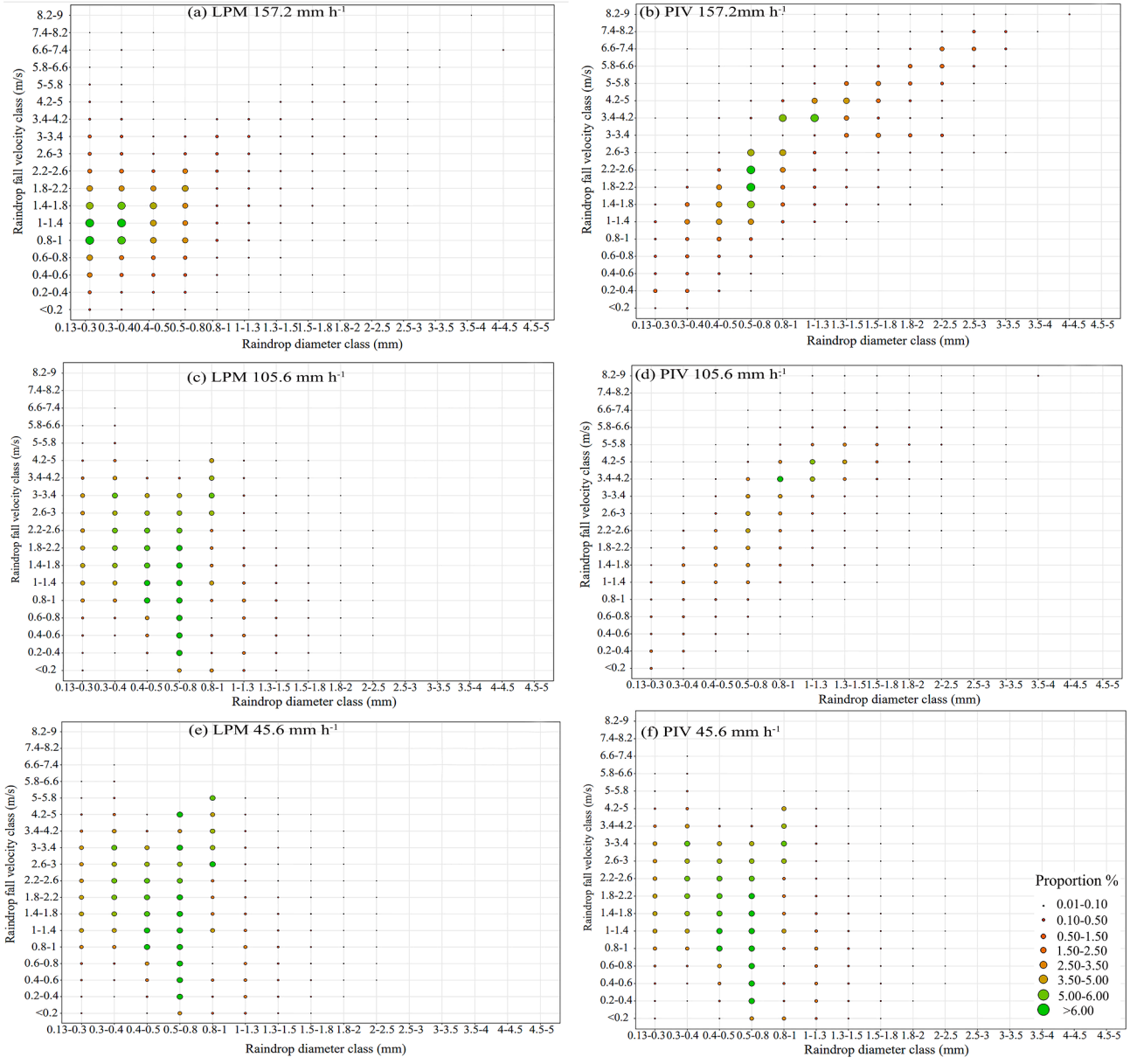

Fig. 7. The raindrop falling velocity proportion measured by LPM and PIV under the same rainfall. The largest rain (157.2 mm h^{-1}), moderate rain (105.6 mm h^{-1}) and lightest rain (45.6 mm h^{-1}) were taken as examples in this experiment. LPM = laser precipitation monitor; PIV = particle imaging visual measurement technology. The sizes and colours of the different circles indicate the proportion of raindrops in each category.

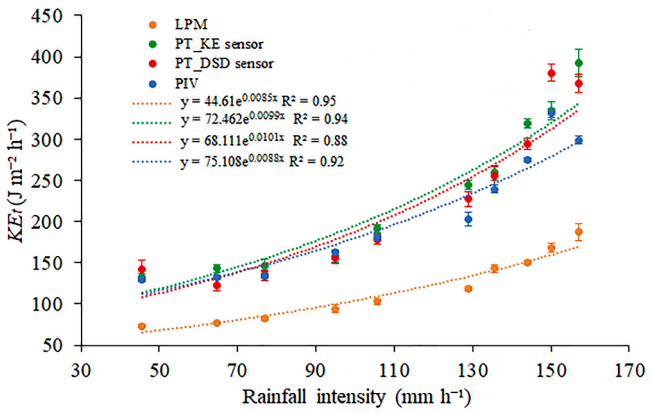

Fig. 8. The rainfall kinetic energy rate (KE_t) measured by the three instruments changes with the rainfall intensity. Note: KE_t of the particle imaging visual measurement technology (PIV) is calculated by using Eq. (7). Note: LPM = laser precipitation monitor; PT-KE sensor = KE sensor of piezoelectric transducer; PT-DSD sensor = DSD sensor of piezoelectric transducer; Bars represent ± standard error.

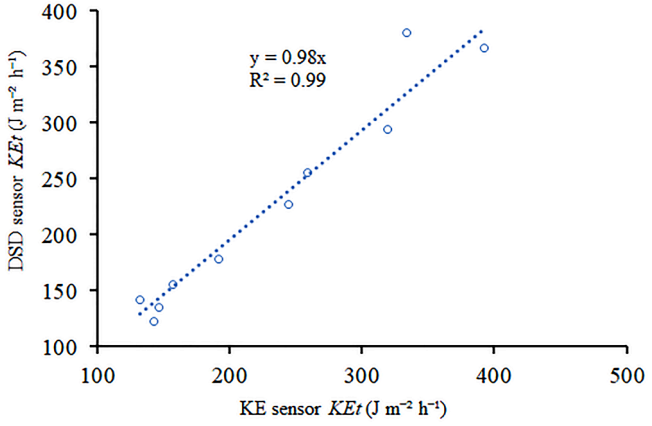

Fig. 9. Relationship between the direct measured mean rainfall kinetic energy rate (KE_t) using the PT-KE sensor and the estimated mean rainfall kinetic energy rate using the PT-DSD sensor. Note: KE sensor (KE_t calculated by using Eq. (2)); DSD sensor (KE_t calculated by using Eqs. (3) and (4)).

that measured by PIV (Fig. 10c). The KE_t measured by the LPM was approximately 0.51 times that measured by PT (Fig. 10d, e). This result indicates that under the same rainfall event, the KE_t measured by the PT and that measured by PIV were similar and greater than that measured by the LPM.

4. Discussion

4.1. DSD and fall velocity measured by LPM, PT and PIV

The differences in the raindrop sizes and fall velocity distributions of LPM, PT, and PIV are due to the differences in instrument design, measurement area, raindrop size and velocity classification, and internal algorithms. Zhan et al.'s (2020) studies demonstrated that PIV was able to reliably detect DSD and raindrop fall velocity for natural rain measurements by assessing the diameter and fall velocity of steel balls and natural raindrops. In this study, it was reasonable that the number of raindrops and sizes measured by LPM and PIV increased with increasing rainfall intensity under simulated rainfall (Table 2). The number of raindrops per unit area measured by the LPM was significantly greater than that of PIV, while the maximum and minimum diameters of raindrops measured by PIV were greater than those of LPM (Table 2). This could be because PIV is based on optical imaging. Thus, some incongruous raindrops are discarded as image noise, and thus, the number of raindrops changes (Zhan et al., 2020), while LPM records discarded incongruous raindrops as real raindrops due to its optical infrared light transmission. Compared to the PIV and PT sensors, the raindrop size measured by the LPM was small (Table 2), which can be attributed to the raindrop diameter measured by the LPM being equal to D_2 (Fig. 5). However, PIV measured the geometric mean diameter, which was greater than D_2. Raindrops of < 1 mm are almost spherical (Lanza et al., 2021), and thus, the raindrop sizes measured by LPM and PIV should be approximately similar. In addition, the LPM sensor with laser optical rats has a better ability to recognize small raindrops (<1 mm). Chang et al. (2020) and Krajewski et al. (2006) reported that optical instruments were sensitive to diameters <0.5 mm. Johannsen et al. (2020) compared the LPM to other sensors and found that the LPM records a high number of small raindrops (<1 mm) and underestimates the raindrop size. Therefore, it not only more sensitive to smaller drops but could also have a bias in its measurement towards smaller drops. Therefore, the raindrop diameter measurement method of LPM needs to be improved. Comparing the raindrop diameter measurement results with the PIV and LPM instruments, it was found that the LPM needs to be calibrated to calculate the D_{50} based on the shape of raindrops measured by PIV. The D_{50} calculated by PIV with the geometric mean diameter was approximately 1.61 times that of the LPM (Table 2). Thus, a value of 1.61 can be used to calibrate the D_{50} calculated by the LPM. Additionally, PT was insensitive to measuring raindrops < 1 mm. This could be ascribed to the fact that PT measured the DSD depending on the change in voltage signal caused by the raindrop impact energy on the sensor surface and cannot accurately measure the number of each size of raindrop. Smaller raindrops (<1 mm) had a lower impact force because of their lighter mass (Meshesha et al., 2016). Thus, the PT was not sensitive to measuring small raindrops (<1 mm), as the sensor was designed to measure rainfall erosivity (Abd Elbasit et al., 2017). The ability of the PT to measure < 1 mm raindrops needs to be further improved. However, the kinetic energy generated by raindrops < 1 mm was very small, and thus, the estimation of rainfall kinetic energy was similar to that of the PIV measurements. In this study, since PT measures the raindrop terminal velocity by using empirical equations (Eq. (4)), only the velocities of raindrops measured by LPM and PIV were compared. The raindrop velocity distributions measured by LPM and PIV were consistent under a rainfall intensity of 45.6 mm h^{-1}, but they still differed form that with a rainfall intensity > 45.6 mm h^{-1} (Fig. 7). As the rainfall intensity increases, the LPM tends to record a large number of < 1 mm raindrops with high velocities, while the raindrop velocity distribution measured by PIV was relatively uniform (Fig. 7). This was consistent with Angulo-Martinez et al.'s (2016) and Johannsen et al.'s (2020) results. This could be attributed to that the PIV sampling area being larger than that of the LPM. The width of the LPM laser beam was small, and the occurrence of edge events was also large. The large raindrops with high fall velocity value broke apart and splashed, creating smaller raindrops with high velocity values on the instrument. Meanwhile, PIV has some inbuilt filtering processes that correct for erroneously measured raindrops. Therefore, PIV has an advantage in measuring raindrop sizes and velocity distributions. For LPM, it is necessary to improve the identification ability of erroneous raindrops and optimize the raindrop diameter calculation method.

4.2. KE_t measured by LPM, PT and PIV

For the same rainfall intensity conditions, the KE_t values measured by PT and PIV were approximately similar and were greater than that those measured by LPM (Figs. 8 and 10). This could be attributed to the fact that the diameters of raindrops measured by PIV were generally greater than that those measured by the LPM (Fig. 6), and the fall velocity of raindrops measured by PIV was also greater than that measured by the LPM for large raindrops (>1 mm). The KE_t directly measured by

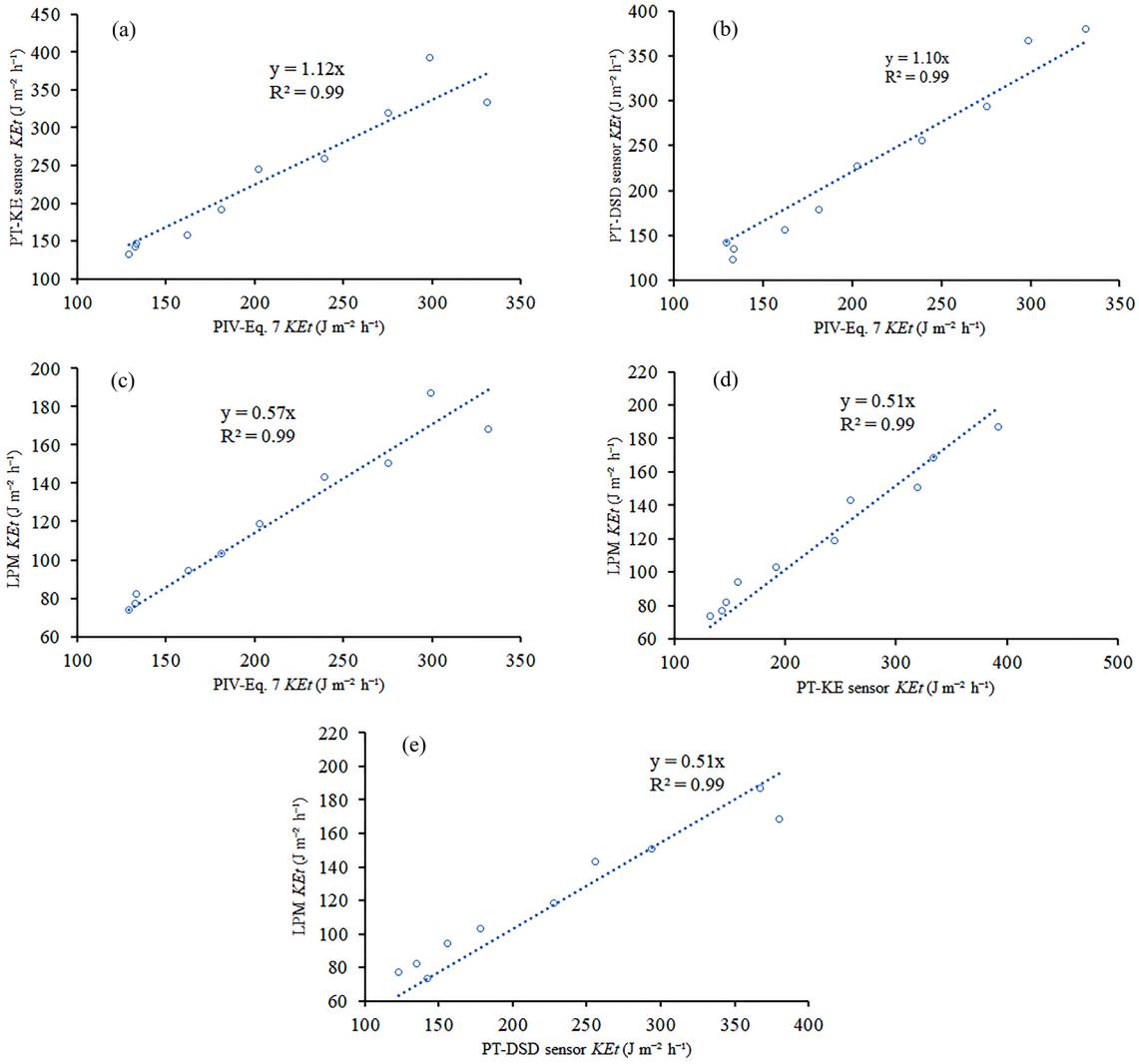

Fig. 10. Intercomparison of the calculated rainfall kinetic energy rate (KE_t) values among the different measuring instruments. Note: PT-KE sensor = KE sensor of a piezoelectric transducer; PT-DSD sensor = DSD sensor of a piezoelectric transducer; LPM = laser precipitation monitor; PIV = particle imaging transient visual measurement technology.

the PT sensor was larger than that measured by the LPM because the PT sensor was more sensitive to the impact energy of large raindrops (>1 mm), which have much higher energy than small raindrops (<1 mm). Although the number of raindrops per unit area measured by the LPM was greater than that measured by PIV (Table 2), the raindrops measured by the LPM were mainly small (<1 mm) (Figs. 6 and 7).

The KE_t values measured by the PT-KE sensor and PT-DSD sensor were significantly correlated (Fig. 9a). The results indicated that it was feasible to calculate the rainfall KE_t by combining the DSD sensor with the empirical velocity equation (Eq. (4)). This was consistent with the results of Abd Elbasit et al. (2011).

To accurate calculation of rainfall KE_t plays an important role in soil erosion prediction (Angulo-Martinez et al., 2016; Carollo et al., 2018; Meshesha et al., 2016). In this study, compared with PIV and PT sensors, LPM underestimated the kinetic energy of the same rainfall. The rainfall KE_t measured by the LPM was approximately 0.57 and 0.51 times that measured by PIV and PT, respectively (Fig. 10), which was reasonable because the diameter and velocity of raindrops measured by LPM were less than those measured by PIV under the same conditions (Table 2; Fig. 7). Therefore, based on the PIV results, the rainfall KE_t measured by the LPM could be calibrated by multiplying by a correction factor of 1.75. However, the value of the correction factor needs to be further verified.

4.3. Errors and applications

Various raindrop sampling areas of different instruments could also lead to different DSD characteristics (Tapiador et al., 2010; Jaffrain et al., 2011). The sampling areas of the three instruments were in the following order: PIV > PT > LPM. In general, larger sampling areas have greater opportunities to collect more representative raindrops (Chang et al., 2020). Meanwhile, a larger sampling area can be used to determine the contemporaneous impact of many raindrops. Compared with previous disdrometers based on line scanners, PIV provided a solution offering a compromised for a nonrepresentative sample limited by a relatively small view size (Zhan et al., 2020). Some measurement errors were also introduced by using LPM and PIV, such as raindrops splashing from the device arm into the sensor and overlapping raindrops (Angulo-Martinez et al., 2016; Chang et al., 2020; Wilken et al., 2018). Moreover, most instruments cannot distinguish betweenmultiple raindrops that cross the sensor at the exact same time (Lanza et al., 2021). The PT sensor had difficulty distinguishing more than two raindrops falling on the sensor synchronously (Abd Elbasit et al., 2010). Although the shell surface of the PT sensor is designed to be convex, the water film formed on the PT sensor surface still reduces its response to raindrop impacts and results in the underestimation of KE_t under very high rainfall intensities. The PT is less affected by the raindrop shape because kinetic

energy depends only on the raindrop mass and fall velocity but can still affect energy transfer upon impact. The LPM instrument interpreted simultaneous raindrops as one single raindrop with a larger diameter that moves faster than a real raindrop of the same diameter, which could potentially result in overestimation of the raindrop size and kinetic energy. Additionally, the raindrop diameter measured by LPM was equal to the minor axes of raindrop, D_2 (Fig. 5). As the rainfall intensity and raindrop size increased, the major axes of raindrops, D_1, increased, and the minor axes of raindrops, D_2, decreased (Lanza et al., 2021). The LPM systematically underestimates the raindrop diameter with respect to PIV, leading to an underestimation of the calculated rainfall kinetic energy. Therefore, LPM greatly underestimates the raindrop size with the increasing rainfall intensity and raindrop size. PIV can directly measure the exact shape and size of precipitation particles. Meanwhile, PIV decreased the length of time required for image processing and increased the image quality. The raindrops measurements taken by the LPM need to be improved when measuring raindrop diameters based on real raindrop shapes measured by PIV.

5. Conclusions

Three instruments, a laser precipitation monitor (LPM), piezoelectric transducer (PT), and particle imaging transient visual measurement technology (PIV), were simultaneously employed and evaluated to describe the rainfall characteristics under 10 simulated rainfall events with different rainfall intensities. The rainfall kinetic energy rate (KE_t), raindrop size distribution (DSD), and raindrop falling velocity were measured.

The comparisons showed that under the same rainfall conditions, the number of raindrops per unit area measured by an LPM was larger than that measured by PIV for cases with the same rainfall conditions. The number of raindrops per unit area measured by both LPM and PIV increased with increasing rainfall intensity. The raindrop size distribution measured by PIV was more uniform than that of PT and LPM for the same rainfall. This was because the three instruments calculate raindrop diameters differently. The PT was not sensitive to raindrops < 1 mm, as the sensor was designed to measure rainfall erosivity. The geometric mean diameter was a more accurate representation of raindrop size because PIV can capture the true irregular shape of raindrops. The median diameter of raindrops (D_{50}) calculated by PIV with the geometric mean diameter was on average 1.61 times that of LPM. For raindrop sizes > 1 mm, the LPM can be calibrated based on the work of PIV. As the simulated rainfall intensity increases, the falling velocity of raindrops < 1 mm measured by PIV was smaller than that measured by LPM. This study revealed that the three instruments with different measuring principles provided different raindrop size distribution measurements, but the PIV and PT results were approximately the same when measuring rainfall kinetic energy for the same rainfall conditions. The KE_t calculated by LPM was 0.51 and 0.57 times that of PIV and PT, respectively. A correction factor of 1.75 could provide a reference for the calibration of the kinetic energy calculation of LPM instruments. Moreover, PIV instruments can be recommended for measuring raindrop characteristics based on the comparison measurements results of DSD and raindrop kinetic energy. PIV provides insight into the raindrop shape because it can directly measure each raindrop shape and falling velocity, as optical imaging automeasurement system technology has high precision. On the other hand, the raindrop size ranges measured by PIV were more representative due to the large sampling area of PIV.

Although this study was carried out under limited experimental conditions, it can provide scientific insights for the comparison of optical and impact disdrometer instruments and the calibration of noncatching instruments.

CRediT authorship contribution statement

Enshuai Shen: Methodology, Conceptualization, Formal analysis, Investigation, Writing – original draft. **Gang Liu:** Methodology, Conceptualization, Funding acquisition, Writing – review & editing, Supervision. **Mohamed A.M. Abd Elbasit:** Methodology, Conceptualization, Writing – review & editing, Investigation. **Xiaoyun Zhan:** Conceptualization, Investigation. **Qian Feng:** Investigation. **Chenxi Dan:** Investigation. **Hongqiang Shi:** Investigation. **Xiangyu Chen:** Investigation. **Qiong Zhang:** Investigation. **Zhen Guo:** Investigation.

Declaration of Competing Interest

The authors declare that they have no known competing financial interests or personal relationships that could have appeared to influence the work reported in this paper.

Acknowledgements

This research was jointly supported by the Strategic Priority Research Program of the Chinese Academy of Sciences (No. XDA28010201), the Water Conservancy Science and Technology Innovation Project in Guangdong Province of China (No. 2020-21), the Central Government to Guide Local Scientific and Technological Development Project (No. 2021ZY0023), and the National Research Foundation of South Africa (110771). Raw datasets for this research are available in Mendeley Data at https://doi.org/10.17632/tkbt22634z.1

References

Adolf Thies, Co, K.G., 2011. Laser Precipitation Monitor. Instruction for Use, Thies Clima.
Abd Elbasit, M.A.M., Yasuda, H., Salmi, A., Anyoji, H., 2010. Characterization of rainfall generated by dripper-type rainfall simulator using piezoelectric transducers and its impact on splash soil erosion. Earth Surf. Process. Landf. 35, 466–475. https://doi.org/10.1002/esp.1935.
Abd Elbasit, M.A.M., Yasuda, H., Salmi, A., 2011. Application of piezoelectric transducers in simulated rainfall erosivity assessment. Hydrol. Sci. J. 56, 187–194. https://doi.org/10.1080/02626667.2010.546359.
Angulo-Martinez, M., Begueria, S., Kysely, J., 2016. Use of disdrometer data to evaluate the relationship of rainfall kinetic energy and intensity (KE-I). Sci. Total Environ. 568, 83–94. https://doi.org/10.1016/j.scitotenv.2016.05.223.
Abd Elbasit, M.A.M., Chirima, G.J., Knight, J., 2017. Comment on: Evaluation of kinetic energy and erosivity potential of simulated rainfall using laser precipitation monitor, by Meshesha et al. (2016). CATENA 156, 401–404.
Bassette, C., Bussière, F., 2008. Partitioning of splash and storage during raindrop impacts on banana leaves. Agr. Forest Meteorol. 148, 991-1004. https://doi.org/doi:10.1016/j.agrformet.2008.01.016.
Carollo, F.G., Ferro, V., Serio, M.A., 2016. Estimating rainfall erosivity by aggregated drop size distributions. Hydrol. Process. 30(13), 2119-2128. https://doi.org/doi:10.1002/hyp.10776.
Carollo, F.G., Ferro, V., Serio, M.A., 2017. Reliability of rainfall kinetic power-intensity relationships. Hydrol. Process. 31 (6), 1293–1300.
Carollo, F.G., Serio, M.A., Ferro, V., Cerda, A., 2018. Characterizing rainfall erosivity by kinetic power-Median volume diameter relationship. Catena 165, 12-21. https://doi.org/10.1016/j.catena.2018.01.024.
Chang, W., Lee, G., Jou, B., Lee, W., Lin, P., Yu, C., 2020. Uncertainty in measured raindrop size distributions from four types of collocated instruments. Remote Sens. 12, 1167. https://doi.org/10.3390/rs12071167.
Guillermo, M., Eduardo Federico, T., Fernando, G., 2016. A comparison of two optical precipitation sensors with different operating principles: The PWS100 and the OAP-2DP. Atmos. Res. 178–179, 550–558. https://doi.org/10.1016/j.atmosres.2016.05.007.
Fornis, R.L., Vermeulen, H.R., Nieuwenhuis, J.D., 2005. Kinetic energy-rainfall intensity relationship for Central Cebu, Philippines for soil erosion studies. J. Hydrol. 300, 20–32. https://doi.org/10.1016/j.jhydrol.2004.04.027.
Frasson, R., Krajewski, W.F., 2011. Characterization of the drop-size distribution and velocity-diameter relation of the throughfall under the maize canopy. Agr. Forest Meteorol. 151(9), 1244-1251. https://doi.org/doi:10.1016/j.agrformet.2011.05.001.
Fischer, F., Hauck, J., Brandhuber, R., Weigl, E., Maier, H., Auerswald, K., 2016. Spatio-temporal variability of erosivity estimated from highly resolved and adjusted radar rain data (RADOLAN). Agr. Forest Meteorol. 223, 72–80. https://doi.org/10.1016/j.agrformet.2016.03.024.
Guo, M., Zhan, X., Zhao, J., Lin, Q., 2015. Measurement of raindrop physical properties with particle imaging measurement technology. Trans. Chin. Soc. Agric. Mach. 46, 144–150 in Chinese, with English abstract.
Hu, W., Zheng, F., Bian, F., 2016. The directional components of splash erosion at different raindrop kinetic energy in the Chinese Mollisol Region. Soil Sci. Soc. Am. J. 80, 1329–1340. https://doi.org/10.2136/sssaj2016.03.0066.
Joss, J., Waldvogel, A., 1967. A raindrop spectrograph with automatic analysis. Pure Appl. Geophy. 68, 240–246.

Jaffrain, J., Studzinski, A., Berne, A., 2011. A network of disdrometers to quantify the small-scale variability of the raindrop size distribution. Water Resour. Res. 47, W00H06. https://doi.org/10.1029/2010wr009872.

Johannsen, L., Zambon, N., Strauss, P., Dostal, T., Neumann, M., Zumr, D., Cochrane, T., Klik, A., 2020. Impact of disdrometer types on rainfall erosivity estimation. Water 12, 96. https://doi.org/10.3390/w12040963.

Kruger, A., Krajewski, W.F., 2002. Two-Dimensional Video Disdrometer: A Description. J. Atmos. Ocean. Technol. 19, 602–617. https://doi.org/10.1175/1520-0426(2002)019<0602:tdvdad>2.0.co;2.

Krajewski, W.F., Kruger, A., Caracciolo, C., Golé, P., Barthes, L., Creutin, J.-D., Delahaye, J.-Y., Nikolopoulos, E.I., Ogden, F., Vinson, J.-P., 2006. DEVEX-disdrometer evaluation experiment: Basic results and implications for hydrologic studies. Adv. Water Resour. 29 (2), 311–325.

Loffler-Mang, M., Joss, J., 2000. An Optical Disdrometer for Measuring Size and Velocity of Hydrometeors. J. Atmos. Ocean. Technol. 17, 130–139. https://doi.org/10.1175/1520-0426(2000)017<0130:aodfms>2.0.co;2.

Lanza, L.G., Stagi, L., 2008. Certified accuracy of rainfall data as a standard requirement in scientific investigations. Adv. Geosci. 16, 43–48. https://doi.org/10.5194/adgeo-16-43-2008.

Liu, X., He, B., Zhao, S., Hu, S., Liu, L., 2019a. Comparative measurement of rainfall with a precipitation micro-physical characteristics sensor, a 2D video disdrometer, an OTT PARSIVEL disdrometer, and a rain gauge. Atmos. Res. 229, 100–114. https://doi.org/10.1016/j.atmosres.2019.06.020.

Liu, G., Zheng, F., Jia, L., Jia, Y., Zhang, X., Hu, F., Zhang, J., 2019b. Interactive effects of raindrop impact and groundwater seepage on soil erosion. J. Hydrol. 578, 124066. https://doi.org/10.1016/j.jhydrol.2019.124066.

Lanza, L.G., Merlone, A., Cauteruccio, A., Chinchella, E., Stagnaro, M., Dobre, M., Garcia Izquierdo, M.C., Nielsen, J., Kjeldsen, H., Roulet, Y.A., Coppa, G., Musacchio, C., Bordianu, C., Parrondo, M., 2021. Calibration of non-catching precipitation measurement instruments: A review. Meteorol. Appl. 28 (3), e2002.

Meshesha, D.T., Tsunekawa, A., Tsubo, M., Haregeweyn, N., Tegegne, F., 2016. Evaluation of kinetic energy and erosivity potential of simulated rainfall using Laser Precipitation Monitor. Catena 137, 237–243. https://doi.org/10.1016/j.catena.2015.09.017.

Ma, Y., Ni, G., Chandra, C.V., Tian, F., Chen, H., 2019. Statistical characteristics of raindrop size distribution during rainy seasons in the Beijing urban area and implications for radar rainfall estimation. Hydrol. Earth Syst. Sci. 23, 4153–4170. https://doi.org/10.5194/hess-23-4153-2019.

Park, S.W., Mitchell, J.K., Bubenzern, G.D., 1983. Rainfall characteristics and their relation to splash erosion. Trans. ASAE 26, 795–804. https://doi.org/10.13031/2013.34026.

Sharma, P.P., Gupta, S.C., Foster, G.R., 1995. Raindrop-induced soil detachment and sediment transport from interrill areas. Soil Sci. Soc. Am. J. 59, 727–734. https://doi.org/10.2136/sssaj1995.03615995005900030014x.

Salles, C., Creutin, J.-D., Sempere-Torres, D., 1998. The Optical Spectropluviometer Revisited. J. Atmos. Ocean. Technol. 15, 1215–1222. https://doi.org/10.1175/1520-0426(1998)015<1215:TOSR>2.0.CO;2.

Salles, C., Poesen, J., Semperetorres, D., 2002. Kinetic energy of rain and its functional relationship with intensity. J. Hydrol. 257, 256–270. https://doi.org/10.1016/S0022-1694(01)00555-8.

Szakall, M., Diehl, K., Mitra, S., Borrmann, S., 2009. A wind tunnel study on the shape, oscillation, and internal circulation of large raindrops with sizes between 2.5 and 7.5 mm. J. Atmos. Sci. 66, 755–765. https://doi.org/10.1175/2008jas2777.1.

Shin, S., Park, S., Choi, B., 2016. Universal power law for relationship between rainfall kinetic energy and rainfall intensity. Adv. Meteorol. 2494681, 1–11. https://doi.org/10.1155/2016/2494681.

Serio, M.A., Carollo, F.G., Ferro, V., 2019. Raindrop size distribution and terminal velocity for rainfall erosivity studies. A review. J. Hydrol. 576, 210–228.

Stagnaro, M., Cauteruccio, A., Lanza, L.G., Chan, P.-W., 2021. On the use of dynamic calibration to correct Drop Counter Rain Gauge measurements. Sensors 21, 6321. https://doi.org/10.3390/s21186321.

Shen, E., Liu, G., Jia, Y., Dan, C., Abd Elbasit, M.A.M., Liu, C., Gu, J., Shi, H., 2021a. Effects of raindrop impact on the resistance characteristics of sheet flow. J. Hydrol. 592, 125767. https://doi.org/10.1016/j.jhydrol.2020.125767.

Shen, E., Liu, G., Dan, C., Shu, C., Wang, R., Liu, X., Zhou, J., Chen, X., 2021b. Combined effects of rainfall and flow depth on the resistance characteristics of sheet flow on gentle slopes. J. Hydrol. 603, 127112. https://doi.org/10.1016/j.jhydrol.2021.127112.

Tokay, A., Kruger, A., Krajewski, W., 2001. Comparison of drop size distribution measurements by impact and optical disdrometers. J. Appl. Meteorol. 40, 2083–2097. https://doi.org/10.1175/1520-0450(2001)040<2083:CODSDM>2.0.CO;2.

Tapiador, F.J., Checa, R., de Castro, M., 2010. An experiment to measure the spatial variability of rain drop size distribution using sixteen laser disdrometers. Geophys. Res. Lett. 37 (16), n/a–n/a.

Van Dijk, A., Bruijnzeel, L., Rosewell, C., 2002. Rainfall intensity-kinetic energy relationship: a critical literature appraisal. J. Hydrol. 261, 1–23. https://doi.org/10.1016/S0022-1694(02)00020-3.

Wilken, F., Baur, M., Sommer, M., Deumlich, D., Bens, O., Fiener, P., 2018. Uncertainties in rainfall kinetic energy-intensity relations for soil erosion modelling. Catena 171, 234–244. https://doi.org/10.1016/j.catena.2018.07.002.

Xiao, H., Liu, G., Abdelbasit, M.A., Zhang, X., Liu, P.L., Zheng, F., Zhang, J., Hu, F., 2017. Effects of slaking and mechanical breakdown on disaggregation and splash erosion. Eur. J. Soil Sci. 68, 797–805. https://doi.org/10.1111/ejss.12482.

Zhang, R., Cao, Y., 2010. Research overview of rain effect on aircraft aerodynamic performance. Journal of Aerospace. Power 25, 2290–2295 in Chinese, with English abstract.

Zhan, X., Guo, M., Zhao, J., Shi, H., Shui, J., 2018. Microphysical features of raindrop and rainfall energy based on particle imaging transient measurement technology. Trans. Chin. Soc. Agric. Eng. 34, 107–113 in Chinese, with English abstract.

Zhan, X., Zhao, J., Feng, Q., Shui, J., Guo, M., 2020. Particle imaging auto-measurement system for microphysical characteristics of raindrops in natural rain. Atmos. Res. 242, 104963. https://doi.org/10.1016/j.atmosres.2020.104963.